

## Effects of the surface Miller index on the resonant neutralization of hydrogen anions near Ag surfaces

Himadri Chakraborty,<sup>\*</sup> Thomas Niederhausen, and Uwe Thumm<sup>†</sup>

*James R. Macdonald Laboratory, Department of Physics, Kansas State University, Manhattan, Kansas 66506-2604*

(Received 22 January 2004; published 12 May 2004)

We compare the resonant neutralization dynamics of hydrogen anions in front of plane Ag surfaces of symmetries (100) and (111) using a Crank–Nicholson wave-packet propagation method. For the Ag(100) surface, the surface state, degenerate with the valence band, rapidly decays while being populated by the ion. For Ag(111), in contrast, the population of a quasi-local Shockley surface state inside the projected  $L$ -band gap impedes the electron decay into the bulk along the direction normal to the surface. This difference in the decay pattern strongly affects the survival of 1 keV ions scattered from these surfaces. Scattering off the Ag(111) surface results in about an order of magnitude higher ion-survival as a function of the exit angle with respect to the surface plane compared to that off Ag(100). Results for Ag(111) show good agreement with measurements [Guillemot and Esaulov, *Phys. Rev. Lett.* **82**, 4552 (1999)].

DOI: 10.1103/PhysRevA.69.052901

PACS number(s): 79.20.Rf, 34.70.+e, 73.20.At

### I. INTRODUCTION

Electron transfer processes between an atomic or a molecular ion and a surface of a metal or a semiconductor are important in several branches of physics and chemistry. Since the electron affinity of the atomic anions is sufficiently higher than the typical Fermi energy of most FCC-metal surfaces, the transfer of electrons from the ion to the surface is predominantly of single-electron nature. This process of resonant charge transfer (RCT) can be characterized as the tunneling of the electron through a potential barrier formed by the ion and the bulk-vacuum interface of the surface. RCT in ion-surface collisions is an intermediate mechanism in complex phenomena related to the development of ion sources, plasma-wall interactions, secondary ion mass spectroscopy, and reactive ion etching [1,2]. Innovations, such as semi-conductor miniaturization, are driven by advances in thin-film-deposition techniques where inherent surface-chemical reactions involve the RCT process.

A few years ago, it was predicted [3,4] and experimentally confirmed [5] that RCT in ion-surface interactions is strongly influenced by the projected band gap of the crystal along the surface normal. This happens because the gap prevents electron penetration normal to the surface, which is the favorable direction for RCT. On the other hand, a variation in the crystallographic symmetry of the surface can alter the substrate electronic structure to a large extent while the band gap may still exist. This can considerably influence the transfer dynamics which is shown in an extensive study of  $H^-$  ions impinging on Cu surfaces of symmetries (111) and (100) [6]. In this study, the ion velocity was considered slow enough to approximate adiabatic conditions. As a result, the difference between (111) and (100) surface state electronic structure was found to be important for intermediate ion surface distances, approximately, between 3 and 8 a.u. For

closer distances, the adiabatic ion affinity level shifts towards the vacuum energy. This was found to result in a strong decay near the (111) surface through the conduction band and a loss of electrons near the (100) surface via population of image states.

We consider fast  $H^-$  ions with an incident kinetic energy of 1 keV in the present study, since measurements [5] are available at this beam energy. Further, energetic ions ensure shorter ion-surface effective interaction times. This will help understand dynamical effects as a deviation from pure adiabatic collisions. A comparative study of two silver surfaces of differing Miller indices (111) and (100) is made for the first time, and the calculated ion-survival probability in collisions with Ag(111) is compared with the experiment [5].

Over the years, a number of nonperturbative methods have been employed to investigate the RCT process theoretically. These include single-center basis-set-expansion [7], complex coordinates rotation [8], two-center expansion [9], multi-center expansion techniques [10], and the direct numerical integration of the effective single-electron Schrödinger equation by Crank–Nicholson wave-packet propagation (CNP) [3,4,6,11,12]. Of all these methods, CNP has an important flexibility in practical applications, besides being mathematically more exact. It can readily be applied to any effective potential that may be used to represent the electronic structure of substrate and projectile. As a result, in contrast to usual expansion methods that simplify the target to a free-electron (jellium) metal, CNP can incorporate a significantly more detailed representation of the substrate structure. Therefore, in this method, the influence of band gaps [3,5], surface states, and image states on the RCT dynamics can be addressed more directly and conveniently.

We use a CNP methodology to perform our calculations. In the following section, we describe potentials and some essential aspects of the theory. The subsequent section presents a discussion of our results. We summarize and make concluding remarks in the final section. Unless stated otherwise, we use atomic units.

<sup>\*</sup>Email address: himadri@phys.ksu.edu

<sup>†</sup>Email address: thumm@phys.ksu.edu

## II. POTENTIALS AND PROPAGATION

We model the Ag(100) and Ag(111) surface by a one-dimensional (1-d) [in the co-ordinate ( $z$ ) along the surface normal] semi-empirical single-electron effective potential, constructed from pseudopotential local density calculations [13]. This potential has the following analytic form:

$$V_{\text{surf}}(z) = V_1(z) + V_2(z) + V_3(z) + V_4(z), \quad (1)$$

where

$$V_1(z) = A_{10} + A_1 \cos\left(\frac{2\pi}{a_s}z\right), \quad z < 0, \quad (2a)$$

$$V_2(z) = -A_{20} + A_2 \cos[\beta z], \quad 0 < z < z_1, \quad (2b)$$

$$V_3(z) = A_3 \exp[-\alpha(z - z_1)], \quad z_1 < z < z_{\text{im}}, \quad (2c)$$

$$V_4(z) = 27.21 \text{eV} \frac{\exp[-\lambda(z - z_{\text{im}})] - 1}{4(z - z_{\text{im}})}, \quad z_{\text{im}} < |z|. \quad (2d)$$

The Ag atomic layers are separated by the lattice constant  $a_s$  [ $=3.853a_0$  for Ag(100) and  $=4.430a_0$  for Ag(111)]. The top-most layer of lattice points defines  $z=0$ . Following Ref. [13], the sets of four independent parameters in Eqs. (2) for both surfaces are

	$A_{10}(\text{eV})$	$A_1(\text{eV})$	$A_2(\text{eV})$	$\beta(a_0^{-1})$
Ag(100)	-9.30	5.04	3.8808	2.4222
Ag(111)	-9.64	4.30	3.8442	2.5649

The remaining six parameters are determined by making the logarithmic derivative of the potential continuous everywhere in space. The parameter  $z_{\text{im}}$ , that defines the image plane position, thus becomes  $2.064a_0$  for Ag(100) and  $2.216a_0$  for Ag(111).

These potentials yield very different electronic structures for the surfaces. (All the energies in the spectrum are expressed with respect to the vacuum energy.) The Ag(100) surface has the bottom of a projected  $X$ -band gap at  $-2.92$  eV, but the gap extends beyond the vacuum energy up to  $2.14$  eV. There occurs a surface state at  $-3.05$  eV that is degenerate with the valence band. The Ag(100) potential also supports a Rydberg series of image states inside the band gap. The energies of the first two image states are  $E_1 = -0.53$  eV and  $E_2 = -0.17$  eV. For Ag(111), a projected  $L$ -band gap exists between  $-0.6$  and  $-5.0$  eV. A surface state at  $-4.56$  eV occurs inside this gap. The first image state at  $E_1 = -0.77$  eV lies just below the upper edge of the band gap while higher image states are degenerate with the conduction band.

A spherically symmetric effective single-electron potential is used to describe the  $\text{H}^-$  ion [14]. The potential models the interaction of the active electron with a polarizable core. A regularized version of this potential [15],

$$V_{\text{ion}} = \frac{\gamma U}{\sqrt{\mu U^2 + 1}}, \quad (3)$$

where

$$U(r) = -(1 + 1/r)\exp(-2r) - (a/2r^4)\exp(-b/r^2), \quad (4)$$

is employed to ensure good numerical accuracy for small radial co-ordinates. Here  $r$  denotes the distance from the hydrogen core, whose polarizability  $a$  is  $4.5$ . The parameter  $b$  is set to  $2.547$ . On a 3-d grid ( $r = \sqrt{x^2 + y^2 + z^2}$ ),  $\mu = 0.1156$  and  $\gamma = 1.107$  yield an electron affinity of  $0.76$  eV [15]. However, to suit our reduced-dimensionality calculations, we reparametrized  $\mu$  and  $\gamma$  ( $\mu = 0.1417$ ,  $\gamma = 0.3923$ ) for a 2-d  $\text{H}^-$  ion in order to ensure the same electron affinity.

CNP [11,12] is applied on the initial unperturbed  $\text{H}^-$  wave function  $\phi_{\text{ion}}(\vec{r})$ . The propagation is carried out over a 2-d numerical grid in which the metal continuum is approximated by free electronic motion in the  $x$  direction, parallel to the surface. This renders the surface translationally invariant in the parallel direction. The time-dependent electronic wave function  $\Phi(\vec{r}, t)$  is a solution of the time-dependent Schrödinger equation with the Hamiltonian

$$H = H' + H_{\text{free}}, \quad (5)$$

where

$$H' = -\frac{1}{2} \frac{d^2}{dz^2} + V_{\text{ion}} + V_{\text{surf}}, \quad (6a)$$

$$H_{\text{free}} = -\frac{1}{2} \frac{d^2}{dx^2}. \quad (6b)$$

For fixed ion-surface distances  $D$ , the Hamiltonian (5) is time-independent (static case). The corresponding propagation over time  $t$  yields

$$\Phi(\vec{r}, t + \Delta t; D) = \exp[-iH(D)\Delta t]\Phi(\vec{r}, t; D), \quad (7)$$

where the initial wave packet  $\Phi(\vec{r}, t=0; D) = \phi_{\text{ion}}(\vec{r}; D)$ . We approximate the time evolution operator by the split operator expression

$$\begin{aligned} \exp(-iH\Delta t) &\approx \exp(-iH_{\text{free}}\Delta t/2)\exp(-iH'\Delta t) \\ &\times \exp(-iH_{\text{free}}\Delta t/2). \end{aligned} \quad (8)$$

The unitary and unconditionally stable Cayley scheme [11] is used to evaluate the exponential operators in Eq. (8).

We construct a grid which includes 100 atomic layers of bulk and extends to  $z=100$  on the vacuum side. This represents well the important surface and bulk properties along the  $z$  direction. The grid extends from  $x=-120$  to  $x=120$  in the parallel direction. The operators are discretized over this grid using a three-point differentiation formula, and the Crank–Nicholson algorithm is applied via diagonalization of a tridiagonal matrix in order to obtain  $\Phi(\vec{r}, t)$  at every time step [11]. Grid spacings  $\Delta z=0.2$  and  $\Delta x=0.3$  were found to be adequate.

At each time step, the ionic survival amplitude (autocorrelation) is calculated as the overlap

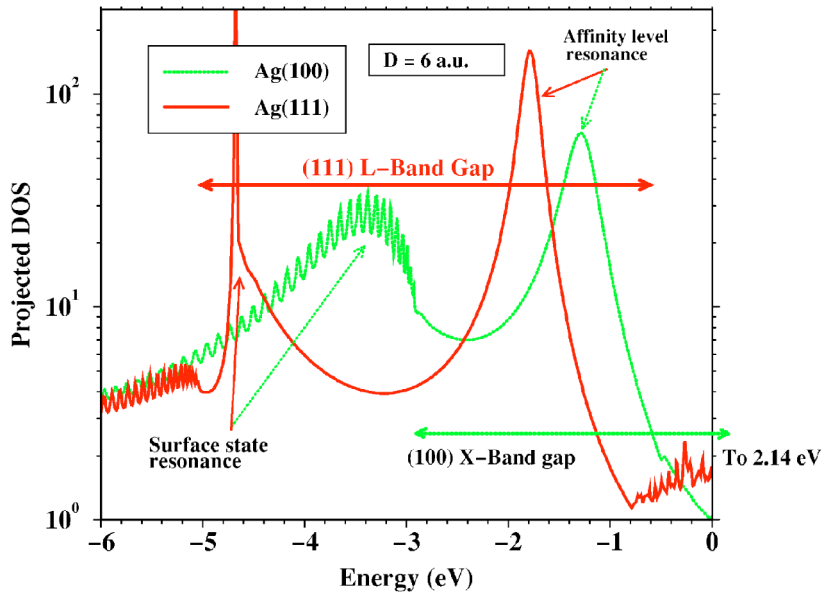


FIG. 1. (Color online) The projected density of states at the ion-surface separation  $D=6$  a.u. for Ag(100) and Ag(111) surfaces. The band gaps corresponding to each of the surfaces are indicated as horizontal double-headed arrows. The origin of the energy scale is defined by the vacuum energy.

$$A(t) = \langle \Phi(\vec{r}, t) | \phi_{\text{ion}}(\vec{r}) \rangle. \quad (9)$$

The real part of the Fourier transform (FT) of this amplitude yields the projected density of states (PDOS) that exhibits resonances corresponding to various states populated by the ion. The energy, lifetime, and level of population of these quasi-stationary states are directly obtained by the position, width (FWHM), and amplitude of the resonances. The FT of  $A(t)$  is performed by propagating  $\Phi(\vec{r}, t; D)$  over a period long enough for  $A(t)$  to become practically zero, which implies a total departure of the wave packet from the ion. The resonance energies and widths are found well-converged for time-steps  $\Delta t=0.2$ . We employ appropriate absorbers at the grid edges in order to preempt unphysical reflection of outgoing electron flux from grid boundaries. This enforces the correct outgoing wave behavior of the continuum electrons.

In a scattering scenario, the movement of the ion in front of the surface invokes the time-dependence in the Hamiltonian (dynamic case). Sufficiently close to the surface, the ion gradually decelerates in the normal direction along its incoming trajectory. This is due to the repulsive interaction between the ion-core and all surface atoms collectively. As a result, the normal velocity ( $v_{\text{nor}}$ ) of the ion becomes zero at the point of closest approach ( $D_{\text{cls}}$ ). For specular reflection, the ion regains its original normal velocity. For a given initial asymptotic kinetic energy  $E$  and angle of incidence  $\Theta$  (that is equal to the exit angle), we simulate the classical ion-trajectory by modeling the core-surface interaction via the “Biersack-Ziegler” interatomic potential [16], averaged over a line of Ag atoms along the parallel direction. This defines a  $D_{\text{cls}}$  as a function of the initial normal velocity,  $v_{\text{nor}}^{\text{in}}$ . We did not find that the inclusion of image interaction at large distances is of any significance in the simulation of trajectories [17]. Under our assumption of a translationally invariant surface, the parallel velocity  $v_{\text{par}}$  of the ion remains constant and equal to its asymptotic value. The ionic motion is then incorporated in the electronic wave-packet propagation by adding

appropriate translational phases. This is done by multiplying the wave packet with  $\exp[-i(v_{\text{par}}x + \epsilon v_{\text{nor}}z + v^2t/2)]$ . The parameter  $\epsilon$  is  $\pm 1$  on the incoming and the outgoing part of the trajectory, respectively. We evaluate the ionic survival probability long after the ion’s scattering from the surface as

$$P_{2-d}^{\text{WPP}}(E, \Theta) = \lim_{t \rightarrow \infty} |A(t)|^2, \quad (10)$$

where the subscript 2-d refers to the dimensionality of the model.

### III. RESULTS AND DISCUSSIONS

#### A. Static case: Propagations with a fixed ion

The positions and the widths of resonances in the PDOS, obtained via propagation at fixed ion-surface distances, are important to describe the charge transfer interaction of a moving ion with a surface. This is true even for relatively fast incident ions, because  $v_{\text{nor}}$  at close ion-surface distances becomes so retarded due to the surface repulsion that the transfer dynamics approximates adiabatic conditions. We begin by comparing the resonances in PDOS spectra due to Ag(100) and Ag(111) for two typical ion-surface distances.

Figure 1 shows the PDOS corresponding to  $D=6$  for both Ag(100) (dotted line) and Ag(111) (solid line) surfaces. Our numerical grid extends over a finite section of the substrate. Since the absorption at the grid edge is not complete (even though almost so), very weak resonances corresponding to bulk states appear in the PDOS. These structures correspond to valence band states of the (100), and valence as well as conduction band states of the (111) surface (Fig. 1). The widths of these resonances are due to their free decay in the parallel direction. The positions of the band edges below the vacuum energy are very well reproduced. The affinity level resonances for (100) and (111) surfaces appear at  $-1.29$  and  $-1.79$  eV, and have widths of 0.377 and 0.2 eV, respectively. However, the difference in the character of surface state resonances from one symmetry to the other is very pronounced.

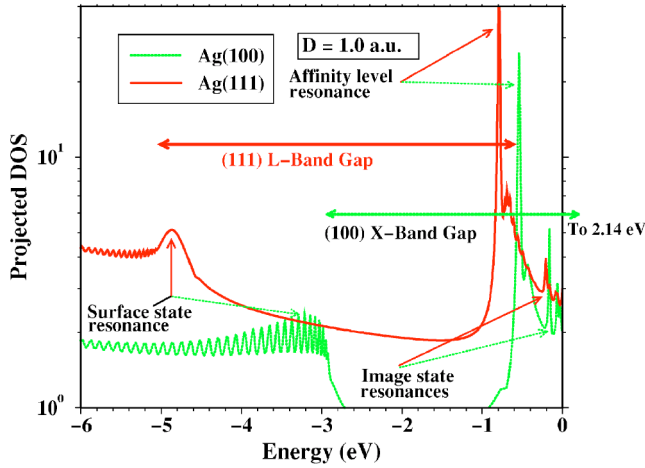


FIG. 2. (Color online) Same as Fig. 1, but for  $D=1$  a.u.

For the (100) surface, this resonance (at  $-3.37$  eV) is embedded in the valence band and, therefore, strongly couples with the bulk along the normal direction. Hence, besides its decay along the free parallel continuum, the (100) surface state suffers an additional decay in the normal direction. In fact, owing to its overlap with a large number of bulk states, the latter channel is much stronger and contributes dominantly to the large width ( $0.863$  eV) of the resonance. In sharp contrast, the (111) surface state lies in the band gap and decays only along the parallel direction, leading to a far narrower width ( $0.022$  eV).

Interestingly, going to  $D=1$  (Fig. 2), the (100) and (111) affinity level resonances (at  $-0.540$  and  $-0.791$  eV, respectively) are narrower than for  $D=6$  and of nearly identical widths ( $0.026$  and  $0.023$  eV, respectively). The surface state resonances are wider at  $D=1$ . For the (111) surface we obtain a width of  $0.330$  eV, while the (100) resonance is so wide that no width can be extracted in Fig. 2. Extra resonance features corresponding to the image states appear just below the vacuum level for both surfaces. This is indicative of the fact that at such a close ion-surface distance the ion affinity level has energetically moved closer to the image states, leading to their population and decay (cf. Figs. 3 and 4). For the (100) surface the image states being inside the band gap decay only into their parallel continua. In contrast, for (111) surfaces, the proximity of the first image state to and the degeneracy of the higher ones with the conduction band open additional channels for these states, allowing decay along the normal direction into the bulk. In order to obtain a complete picture of the interactions among several quasi-stationary states of the ion-surface composite, we present in the following the position and the width of the resonances as a function of  $D$ .

At large distances, the energy (Fig. 3) of the affinity level resonances for (100) (opaque circles) and (111) surfaces (filled circles) as a function of  $D$  are approximately identical and, hence, show no dependence on the surface Miller index. This is because, at these distances, the affinity level shift is solely governed by the image-charge interaction  $\sim -1/(4D)$ , leading to a good agreement with free electron (jellium) results (not shown). However, moving below  $D=10$ , the situ-

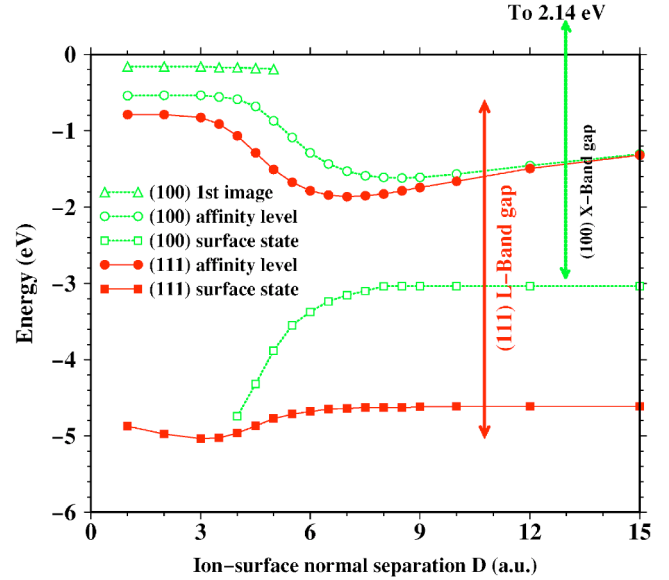


FIG. 3. (Color online) Energies of various resonances as a function of the ion-surface distance for Ag(100) and Ag(111) surfaces.

ation alters. While the (100) affinity level resonance begins to shift upwards at about  $D=8$ , for the (111) surface, this upward shift starts closer to the surface, at  $D \approx 7$ , and leads to a deeper minimum. For either surface, an avoided crossing between the affinity level and the surface state resonance [opaque squares for (100) and filled squares for (111) surfaces] develops. As a result, at smaller values of  $D$ , the (100) affinity level resonance moves to the close vicinity of the image states (the first image state resonance is shown as opaque triangles), enabling interactions of the ion with these states. Likewise, at such small distances, the (111) affinity level resonance moves close to the image states (not shown) and the conduction band. With decreasing  $D$ , the (100) surface state resonance, embedded in the valence band, continues to move deeper in energy from the point of the avoided crossing. On the other hand, the (111) surface state resonance shifts towards the valence band but gets repelled to move upwards below  $D=3$ , forming a minimum. This is due to its interactions with valence band states. In general, this behavior of the resonance position as a function of  $D$  is characterized by the (adiabatic) repulsion between interacting states.

In Fig. 4, at large ion-surface distances, the increase in the width of the affinity level resonances for both surfaces with decreasing  $D$  indicates their increasingly stronger interactions with the corresponding surface state and the associated decay. The (100) surface state has an extremely efficient decay channel along the surface normal due to its coupling with the bulk states. Since this state energetically descends into the valence band with decreasing  $D$  (Fig. 3), the effect of this coupling enhances, resulting in an increase in its width. The turn-around of the (100) affinity level resonance width, forming a maximum around  $D=6$ , is due to the interaction of the respective quasi-stationary state with the surface state through valence band continua. Similarly, a strong interaction between the affinity level and surface state resonance of the (111) surface is evident in the distance-dependent widths at  $D \leq 8$ , where a maximum in the affinity

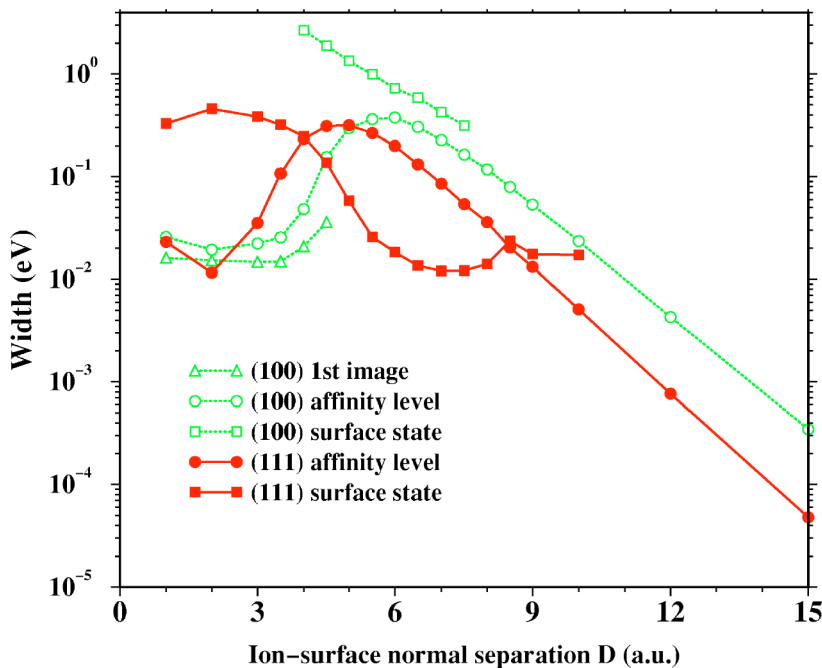


FIG. 4. (Color online) Widths of various resonances as a function of the ion-surface distance for Ag(100) and Ag(111) surfaces.

level resonance width occurs at  $D \approx 4.5$ . This is the consequence of an indirect coupling between the corresponding discrete quasi-stationary states through the surface state continuum. At  $D < 3$  this interaction weakens and the decay via the image state parallel continua for the (100) and via the image states into the metal conduction band for the (111) surface becomes important, as the corresponding energy behavior suggests (Fig. 3). Simultaneously, at these distances, the (111) surface state decays through the valence band. The width of the first image state resonance of the (100) surface seems to follow a similar  $D$ -dependence as that of the corresponding affinity level resonance.

In the following subsection we shall show that these fixed ion propagation results for resonant energies and widths provide a good guideline to diagnose the results for ions moving along a physical trajectory.

### B. Dynamic case: Propagations with a moving ion

We consider  $H^-$  ions with an initial kinetic energy of 1 keV approaching the surface at various angles from an asymptotic distance of 50 a.u. The ions reflect specularly from the surface. At each angle of incidence  $\Theta$  with respect to the surface plane, the survival probability of the ion is calculated.

Physically, the parallel continuum for the interaction is 2-d (along both  $x$  and  $y$  directions in Cartesian co-ordinates). One way to incorporate that is to exploit the cylindrical symmetry for translationally invariant surfaces [4]. On the other hand, the translational invariance ensures symmetric degrees of freedom along  $x$  and  $y$  continua. Therefore, neglecting any interaction between these continua, an alternate approach to the static problem is to conduct the propagation with a 1-d parallel continuum, as in the present case (Sec. III A), and then double the widths of various resonances to approximate the full 3-d result. In a similar calculation [6] for  $H^-$  on

Cu(111) this doubling of the decay-widths from 1-d continuum led to fair agreement with calculations in cylindrical coordinates [4], barring some mismatches originating from slightly different models of the surface potentials used. In the conventional rate-equation approach to the dynamical problem, the survival probability is directly related to the integral of the static ion level width. Considering  $\Gamma(D)$  to be the width for a 1-d continuum, this probability is

$$P_{3-d}^{\text{Rate}}(E, \Theta) = \exp\left(-\int_{\infty}^{D_{\text{cls}}} dD' \frac{2 \times \Gamma(D')}{v_{\text{nor}}^{\text{in}}}\right), \quad (11)$$

where the factor 2 in the exponent comes from the doubling. Obviously, this *doubling* of the width in a rate-equation approach is equivalent to *squaring* the survival probability, Eq. (10), obtained in our model 1-d parallel continuum calculation. Thus, the non-adiabatic ion-survival probability in full dimensionality is then approximated by

$$P_{3-d}^{\text{WPP}}(E, \Theta) = [P_{2-d}^{\text{WPP}}(E, \Theta)]^2, \quad (12)$$

which allows for the comparison with measured ion-fractions of Ref. [5]. We note that the use of (12) instead of the rate-equation based result (11) is consistent with earlier studies [3,4] that showed the inadequacy of the adiabatic model underlying (11) for the accurate *quantitative* prediction of  $H^-$  survival fractions near Cu(111).

Our results in Fig. 5 show the percentage ion-survival. The physical trajectory with a simulated ion-surface retarding potential (as described in Sec. II) is denoted by trajectory-I. Trajectory-II [shown only for (111) surface] denotes the unretarded broken-straight-line trajectory with  $D_{\text{cls}}$  obtained from the corresponding trajectory-I. Over the whole range of  $\Theta$  considered, the  $H^-$  survival probability for both (100) and (111) surfaces generally increases as  $\Theta$  increases. We explain this trend as follows. For a given initial kinetic energy of the projectile,  $v_{\text{nor}}^{\text{in}}$  (displayed in the upper  $x$  axis of

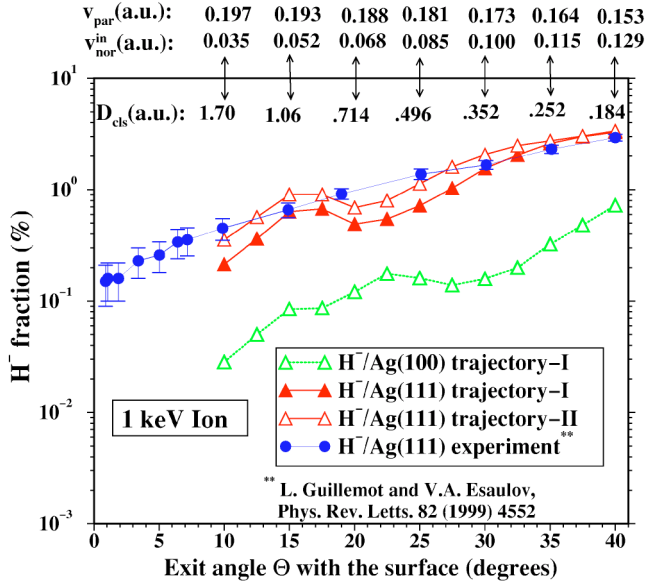


FIG. 5. (Color online) Percentage survival probability [Eq. (12)] of  $H^-$  scattered from Ag(100) and Ag(111) surfaces as a function of the exit angle (= incidence angle for the present case of specular scattering condition) with respect to the surface plane. Initial normal velocities  $v_{\text{nor}}^{\text{in}}$ , constant parallel velocities  $v_{\text{par}}$ , and distances of closest approach  $D_{\text{cls}}$  are given along the upper  $x$ -axis. For the description of trajectory-I and trajectory-II, see the text.

Fig. 5) increases with the increase of  $\Theta$ . This reduces the ion-surface effective interaction time (see Table I, where we define this quantity as the total time the ion spends within  $D \leq 10$ ). Consequently, the levels of population of all substrate states, including the surface state, decrease. This subsequently increases the probability for projectile reionization by these populated states since these states, including the affinity level, cannot decay significantly before the projectile exits the interaction region. Therefore, the larger  $\Theta$  is, the shorter is the interaction time, and, hence, the higher is the ion survival.

The influence of ion retardation on the interaction-time effect can be gauged by looking at the difference between predictions from trajectory-I and trajectory-II for Ag(111) in Fig. 5. For higher  $v_{\text{nor}}^{\text{in}}$ , that is larger  $\Theta$ , this difference is minimal since a significant retardation of the ion can only take place very close to the surface, keeping the effective interaction times along both trajectories comparable (Table I). For decreasing  $v_{\text{nor}}^{\text{in}}$  with decreasing  $\Theta$ , the interaction time in trajectory-I gradually increases relative to trajectory-II. This explains a reduced ion neutralization along trajectory-II for smaller exit angles.

TABLE I. Ion-surface interaction times  $T$ , as defined by the time the ion spends at  $D \leq 10$  a.u., as a function of the angle of incidence  $\Theta$ .

$\Theta$ (deg)	40	35	30	25	20	15	10
$T$ (a.u.):trajectory-I	161	180	206	243	299	388	559
$T$ (a.u.):trajectory-II	153	170	193	224	272	340	478

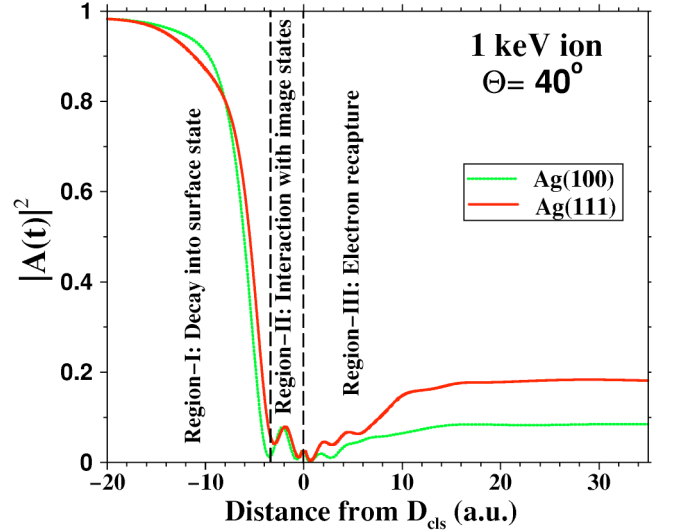


FIG. 6. (Color online)  $|A(t)|^2$  as a function of the distance of the 1 keV ion from the corresponding distance of closest approach  $D_{\text{cls}} = 0.184$  a.u. along trajectory-I; negative and positive distances are respectively the incoming and outgoing segment of the trajectory. The angle of incidence is  $\Theta = 40^\circ$ . Three regions of different interaction characters are identified.

The electron's adiabatic kinetic energy  $E_{\text{KE}}$  in the ion-surface state interaction is the energy difference between the affinity level and the surface state resonances in Fig. 3. On the other hand, an electron in a 1 keV ion can acquire a maximum kinetic energy of 0.55 eV from the ion velocity, suggesting that the interaction is not quite of pure adiabatic character. However, since 0.55 eV is smaller than  $E_{\text{KE}}$  at any  $D$  for either of the surfaces (see Fig. 3), the adiabatic picture partly holds and may still provide a *qualitative* basis of analysis. Hence, a repulsion of the affinity level towards the vacuum energy during the ion's approach to the surface remains. This triggers resonant interactions with image states at close distances. Indeed, we have found the population and decay of image states at such distances by visualizing wave packet probability densities as a function of time along the trajectory. Following our fixed ion results, therefore, different mechanisms of charge-transfer and associated decay dynamics can be approximately identified over three regions of the trajectory: (I) The incoming ion populates primarily the surface state until arriving, roughly, at  $D = 4$  for Ag(100) and  $D = 3$  for Ag(111). The electronic decay, therefore, happens through the respective surface states. (II) Below these distances, until reaching  $D_{\text{cls}}$ , the ion interacts with image states, which are in the band gap for the (100) but coupled with the conduction band for the (111) surface. Electrons, therefore, decay through the parallel continua of (100) image states, but mainly through the (111) conduction band. (III) Along the outgoing part of the trajectory, the dominant process is electron recapture by the nearly depleted ion.

These three regions are shown in Fig. 6, where for a  $40^\circ$  incidence the quantity  $|A(t)|^2$  is plotted against the distance of the ion from  $D_{\text{cls}}$  along trajectory-I. [The results in Fig. 6 are obtained within our 2-d calculation. Note that asymptotic ion-survival probabilities at large (positive) distance are

0.182 and 0.085, respectively, which via Eq. (12) yield corresponding survival probabilities of 3.3% and 0.72% in Fig. 5.] As seen, the effective loss of electrons by the ion is pretty similar for the two surfaces over the first two regions. The final ion survival, therefore, is most sensitively dependent on the extent of recapture in region III. The electronic confinement along the surface normal through the excitation of the quasilocal surface state enables a higher recapture rate for the (111) surface compared to the (100) surface, where the embedded surface state rapidly decays due to its strong coupling with the bulk. On the average, an order of magnitude higher lifetimes of (111) surface states corroborate this (Fig. 4). As a result, the ion survival is significantly higher, approximately by an order of magnitude, near a (111) surface (Fig. 5).

In Fig. 5 we also compare our results with available measurements for  $H^-$  on a Ag(111) surface [5]. In this experiment, the anion fractions were determined by the ratio of the scattered anion flux to the total flux in a given exit angle under specular scattering conditions. The agreement of our results with measurements is quite good at larger  $\Theta$ . For smaller  $\Theta$ , however, the agreement worsens somewhat, but is still reasonable considering the following limitations of the theoretical model: First, results are sensitive to inaccuracies in the classical simulation of the ion trajectory, since the effective interaction time is a crucial determinant of the underlying mechanism. Second, the translational invariance of our model surface potential in the parallel direction limits the dynamics by not including effects related to either the surface corrugation in the parallel direction or the kinematics of the parallel motion [18]. It was experimentally shown [5] that this effect induces an increase in the ion survival already at  $v_{\text{par}}=0.2$ , which is comparable to the  $v_{\text{par}}$  in the present case at smaller  $\Theta$  (see the upper  $x$ -axis of Fig. 5). In this context, we remark that our calculations below  $\Theta=10^\circ$  (not shown) strongly underestimate the measurements. Another limitation of the theory may come from the one-electron character of the model. Multi-electron processes tend to be

relevant for surfaces where RCT is blocked by the projected band gap [19] and by constraints imposed by the Pauli exclusion principle.

#### IV. CONCLUSION

To conclude, evidence for significant electronic excitations to the local surface state in the resonant neutralization of  $H^-$  near Ag(111) is found. In contra-distinction, Ag(100) exhibits a very efficient electronic decay channel through the metal valence band since the (100) surface state has a strong coupling with the bulk. The key to this difference is a highly localizing reflectivity of the (111) projected  $L$ -band gap along the surface normal. For both surfaces the specularly scattered 1 keV ion exhibits qualitatively similar survival. Quantitatively, however, the anion-survival of the (111) surface is much higher since the quasi-local surface state inside the projected band gap retains electrons on the surface to enable their recapture by the ion. Away from grazing incidences ( $\Theta > 10^\circ$ ), our calculations agree with measured reflected ion fractions.

Calculations with a 3-d metal potential having lattice-corrugations in the parallel directions are not expected to qualitatively alter our principal findings, since RCT is largely mediated by transfer along the surface normal. However, by including the parallel velocity effects, such a 3-d potential may bring the ion-survival prediction closer to the experiment. Further, for surfaces which have local structures in the parallel direction [for instance, the (110) surface of the FCC metal with a band gap located at the  $\bar{Y}$  point [20]] a full 3-d potential will be required.

#### ACKNOWLEDGMENTS

This work is supported by NSF (Grant No. PHY-0071035) and the Division of Chemical Sciences, Office of Basic Energy Sciences, Office of Energy Research, US DoE.

- 
- [1] J. P. Gauyacq, A. Borisov, and D. Teillet-Billy, in *Formation/Destruction of Negative Ions in Heavy Particle-Surface Collisions*, edited by V. Esaulov (Cambridge U.P., Cambridge, 1996).
  - [2] H. Shao, D. C. Langreth, and P. Nordlander, in *Low Energy Ion-Surface Interactions*, edited by J. W. Rabalais (Wiley, New York, 1994) p. 118; J. J. C. Geerlings and J. Los, Phys. Rep. **190**, 133 (1990).
  - [3] A. G. Borisov, A. K. Kazansky, and J. P. Gauyacq, Phys. Rev. Lett. **80**, 1996 (1998).
  - [4] A. G. Borisov, A. K. Kazansky, and J. P. Gauyacq, Phys. Rev. B **59**, 10935 (1999).
  - [5] L. Guillemot and V. A. Esaulov, Phys. Rev. Lett. **82**, 4552 (1999).
  - [6] H. S. Chakraborty, T. Niederhausen, and U. Thumm (unpublished).
  - [7] B. Bahrim, D. Teillet-Billy, and J. P. Gauyacq, Surf. Sci. **431**, 193 (1999).
  - [8] P. Nordlander, Phys. Rev. B **46**, 2584 (1992).
  - [9] B. Bahrim and U. Thumm, Surf. Sci. **521**, 84 (2002); P. Kürpick and U. Thumm, Phys. Rev. A **58**, 2174 (1998).
  - [10] F. Martin and M. F. Politis, Surf. Sci. **356**, 247 (1996).
  - [11] W. H. Press, S. A. Teukolsky, W. T. Vetterling, and B. P. Flannery, *Numerical Recipes in FORTRAN* (Cambridge U.P., Cambridge, 1993).
  - [12] U. Thumm, in *Book of Invited Papers, XXII International Conference on Photonic, Electronic, and Atomic Collisions, Santa Fe, NM*, edited by S. Datz *et al.* (Rinton, Princeton, NJ, 2002), p. 592.
  - [13] E. V. Chulkov, V. M. Silkin, and P. M. Echenique, Surf. Sci. **437**, 330 (1999).
  - [14] J. S. Cohen and G. Fiorentini, Phys. Rev. A **33**, 1590 (1986).
  - [15] V. A. Ermoshin and A. K. Kazansky, Phys. Lett. A **218**, 99 (1996).

- [16] J. P. Biersack and J. F. Ziegler, Nucl. Instrum. Methods Phys. Res. **194**, 93 (1982); J. Ducreé, H. J. Andrä, and U. Thumm, Phys. Rev. A **60**, 3029 (1999).
- [17] Image interaction effects on trajectories are only expected to be important for projectiles with higher charge state.
- [18] H. Winter, Comments At. Mol. Phys. **26**, 287 (1991).
- [19] T. Hecht, H. Winter, A. G. Borisov, J. P. Gauyacq, and A. K. Kazansky, Phys. Rev. Lett. **84**, 2517 (2000).
- [20] M. C. Desjonquères and D. Spanjaard, in *Concepts in Surface Physics* (Springer, New York, 1993).